The Initial Fusion Pore Induced by Baculovirus GP64 Is Large and Forms Quickly

Ilya Plonsky and Joshua Zimmerberg

Laboratory of Cellular and Molecular Biosphysics, National Institute of Child Health and Human Development, National Institutes of Health, Bethesda, Maryland 20892-1855

Abstract. The formation of the fusion pore is the first detectable event in membrane fusion (Zimmerberg, J., R. Blumenthal, D.P. Sarkar, M. Curran, and S.J. Morris. 1994. *J. Cell Biol.* 127:1885–1894). To date, fusion pores measured in exocytosis and viral fusion have shared features that include reversible closure (flickering), highly fluctuating semistable stages, and a lag time of at least several seconds between the triggering and the pore opening. We investigated baculovirus GP64–induced Sf9 cell–cell fusion, triggered by external acid solution, using two different electrophysiological techniques: double whole-cell recording (for high time resolution, model-independent measurements), and the more conventional time-resolved admittance recordings. Both methods gave essentially the same results, thus validating the use of the admittance measurements for fusion pore conductance calculations. Fusion was first detected by abrupt pore formation with a wide distribution of initial conductance, centered around 1 nS. Often the initial fusion pore conductance was stable for many seconds. Fluctuations in semistable conductances were much less than those of other fusion pores. The waiting time distribution, measured between pH onset and initial pore appearance, fits best to a model with many (~19) independent elements. Thus, unlike previously measured fusion pores, GP64-mediated pores do not flicker, can have large, stable initial pore conductances lasting up to a minute, and have typical lag times of <1 s. These findings are consistent with a barrel-shaped model of an initial fusion pore consisting of five to eight GP64 trimers that is lined with lipid.

A small pore linking two previously separated aqueous compartments is the smallest structural intermediate that can yet be measured during membrane fusion. In whole-cell patch-clamp recording (Hamill et al., 1981), an increase in cell surface area (as new membrane adds during fusion) is measurable as an increase in cell membrane capacitance (Neher and Marty, 1982). The slow increase in capacitance during the fusion of single large granules in beige mouse mast cells reflects the gradual growth in conductance of an individual fusion pore (Zimmerberg et al., 1987; Breckenridge and Almers, 1987). After opening, exocytotic fusion pores show a wide distribution of conductances ranging from 170 pS to >10 nS, they open and close before securely opening (flicker phenomenon), and they vary in the time course of pore widening between 4 and 400 pS/ms (Fernandez et al., 1984; Zimmerberg et al., 1987; Breckenridge and Almers, 1987; Alvarez de Toledo and Fernandez, 1988; Spruce et al., 1990; Curran et al., 1993). Current discharge through the initial fusion pore can also be measured to calculate its conductance at higher bandwidth (Breckenridge and Almers, 1987; Spruce et al., 1990).

Fusion pores have also been measured for virus-induced cell–cell fusion (Spruce at al., 1989; Lanzrein et al., 1993; Zimmerberg et al., 1994). Influenza hemagglutinin (HA)[1]–mediated fusion pores are similar to exocytotic fusion pores, except flickering is less frequent and the initial fusion pore conductance is smaller (18–375 pS), and pore widening after initial growth at 30–40 pS/ms is temporarily arrested at a conductance of ~600 pS (Spruce et al., 1989, 1991; Tse et al., 1993; Zimmerberg et al., 1994). Initial fusion pores between HA-expressing fibroblasts and planar phospholipid bilayer membranes always flicker, and they have a distribution that is shifted to larger sizes (0.5–4 nS; Melikyan et al., 1995*b*).

As with many enveloped viruses, baculovirus infection leads to early expression of envelope protein (GP64) on the cell surface (Hohmann and Faulkner, 1983; Volkman and Goldsmith, 1984; Keddie and Volkman, 1985). Contacting cells infected by baculovirus will fuse together to

Address all correspondence to Joshua Zimmerberg, Laboratory of Cellular and Molecular Biophysics, National Institute of Child Health and Human Development, National Institutes of Health, 10 Center Drive, MSC 1855, Building 10, Room 10D14, Bethesda, MD 02892. Tel.: (301) 496-6571. Fax: (301) 594-0813. e-mail: joshz@helix.nih.gov

1. *Abbreviations used in this paper*: AM, admittance measurement; DWCR, double whole-cell recording; HA, hemagglutinin; KS, Kolmogorov-Smirnov.

form syncytia when exposed to acid medium (Leikina et al., 1992). Cellular expression of recombinant GP64 also produces pH-dependent syncytia formation (Blissard and Wenz, 1992). Spikes of budded virions are believed to be built of GP64 homooligomers (trimers), and the putative fusion peptide of GP64 is not located in a terminal region (Monsma and Blissard, 1995), as it is in HA (White, 1992).

Membrane fusion is complete soon after the initial pore opens (Curran et al., 1993; Tse and Almers, 1993; Zimmerberg et al., 1994), so it is the initial fusion pore that holds the greatest interest, as differing models of membrane fusion predict very different initial fusion pore structures (Almers and Tse, 1990; Zimmerberg et al., 1991; Nanavati et al., 1992). To measure the initial fusion pore directly, without the model dependence and assumptions of either current discharge or admittance analysis[2], we recorded intercellular (junctional) conductance using double whole-cell recording (DWCR) (Neyton and Trautmann, 1985; Turin et al., 1991; Lanzrein et al., 1993). This method allowed us to control the membrane potential of each cell in a pair independently and to measure the current flowing between them during fusion. Fusion pore conductance data obtained by DWCR were compared to those of admittance measurements (AM).

The initial fusion pore induced by baculovirus *Autographa californica* GP64 has features different from those derived from other cell fusion systems: its conductance is larger; the pore never flickers; and the waiting time between triggering of fusion and pore appearance is very short. Rather than a small gap junction-like channel, we suggest a multisubunit lipid/protein model for this fusion pore that fits both the initial pore conductance and a kinetic analysis of waiting times.

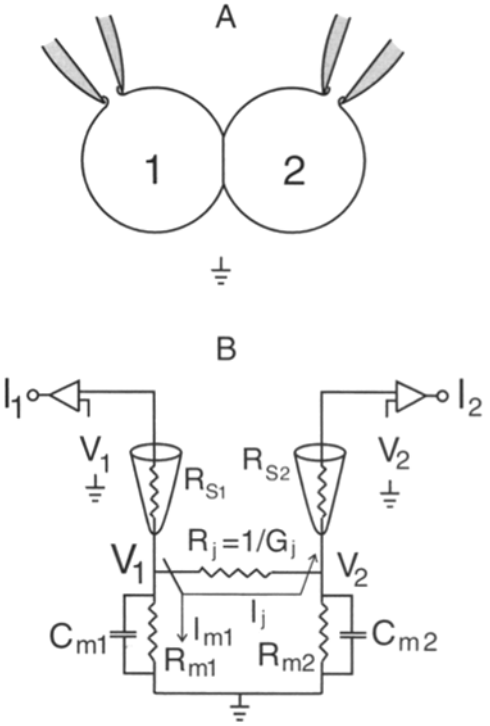

Figure 1. Principles of double whole-cell recording. (*A*) A diagram of the pair of cells. (*B*) Equivalent circuit: R_{s1} and R_{s2}, the series resistances of patch pipettes; R_{m1}, R_{m2}, C_{m1}, and C_{m2}, resistances and capacitances of cells 1 and 2, respectively; R_j, the resistance of the junction between cells. Applying command voltage ΔV_c between cells ($\Delta V_c = V_1 - V_2$) causes two currents to flow from the outputs of patch-clamp amplifiers (I_1 and I_2, respectively). I_1 is equal to the sum of the currents, flowing through nonjunctional (I_{m1}) and junctional (I_j) membranes, while I_2 represents pure junctional current. When I_j is mediated by fusion pore, its conductance can be calculated as $G_p = I_j/\Delta V_c$.

Materials and Methods

Cell Culture

The Sf9 insect cell line, derived from *Spodoptera frugiperda* ovary, and *Autographa caliphornica* multicapsid nuclear polyhedrosis virus were purchased from Invitrogen (San Diego, CA). Cells were grown at 27°C in Grace's medium plus 10% FBS. For infection, monolayers of Sf9 cells in multiwell plates ($\sim 10^6$ cells per well) were incubated with wild-type baculovirus at 10^7 infectious U per ml for 15 min (multiplicity of infection = 3–6 U per cell). Then 0.5 ml of fresh medium were added, and cells were incubated for 36–48 h. Medium was purchased from Invitrogen. All incubations were at 27°C.

Electrophysiological Experiments

For whole-cell recordings, solutions had the following composition (mM): 130 KGlu, 16 KCl, 2 $MgCl_2$, 10 Hepes, 5 EGTA, 50 sucrose, pCa 8 (internal); and 55 NaCl, 10 KCl, 4 $CaCl_2$, 5 $MgCl_2$, 5 glucose, 10 MES, 190 sucrose, pH 6.2 (external). Fusion triggering acid solutions were delivered to cells by slow or fast perfusion, with the same resulting distributions of fusion pore conductance. Acid solution (pH 5.0) used for slow perfusion was identical to the external except for substitution of MES by 10 mM of citric acid. A highly buffered acid solution for fast perfusion contained (mM): 50 sodium citrate, 50 NaCl, 10 KCl, 4 $CaCl_2$, 5 $MgCl_2$, 5 glucose, 20 sucrose, pH 5.0. This acid solution was ejected from a micropipette, placed at about one cell diameter aside a cell pair. Ejections were performed by applying 250-ms pulses of positive pressure (10 psi) into a delivery micropipette using a PV830 Pneumatic Picopump (World Precision Instruments, Sarasota, FL). Patch pipettes had resistances of 1–2 MOhm. For DWCR (see Fig. 1), one cell of each pair was clamped at 0 mV, and the other at −50 mV. Short pulses of voltage (17 ms, −10 mV) were simultaneously superimposed on the holding potentials applied to both cells to monitor the input conductance of each cell in the pair. Currents from the outputs of patch-clamp amplifiers (EPC-7; List Electronics, Darmstadt, Germany) were filtered at 5 KHz with an eight-pole Bessel filter (Frequency Devices, Haverhill, MA) and were acquired at 50 KHz.

For time-resolved AM, a 1-KHz, 50-mV peak-to-peak sine wave was superimposed on the holding potential (−30 mV). Prior compensations of R_{s1} (pipette resistance) and C_{m1} (clamped cell's capacitance) and adjustments of the phase angle were done as described earlier (Joshi and Fernandez, 1988). Sinusoidal current was filtered at 5 KHz, acquired at 40 KHz, and separated "on-line" into imaginary (Im), real (Re), and direct current (G_{DC}) components of the pipette–cell admittance (Y) by a computer program (available upon request). Valve-operating voltage pulse of the Pneumatic Picopump was also acquired and stored together with Re, Im, and G_{DC} data points.

Calculations

Pore Conductance and Radius. In double whole-cell experiments, fusion pore conductance was calculated as junctional conductance $G_p = I_j/\Delta V_c$, where I_j is the transjunctional current (response of cell 2 to the potential

2. Target membrane capacitance and fusion pore conductance are calculated on the basis of cell admittance (for review see Lindau, 1991). This analysis is model dependent: a determination of an appropriate electrical equivalent circuit consistent with the observed changes in cell admittance is required as a first step before values of target membrane capacitance and fusion pore conductance can be calculated. Electrical parameters other than these two are assumed constant or negligible. As the target membrane capacitance must be known, current discharge technique thus includes all assumptions of admittance analysis.

on cell 1) and ΔV_c is a difference between the command potentials of two cells. The accuracy of double whole-cell recording is limited by the fact that ΔV_c is applied to G_j through the series resistances of both recording pipettes (Neyton and Trautmann, 1985). In our experiments, 10 nS approximates an "upper" level below which pore conductances were measured with an accuracy of >90%.

For time-resolved AM, G_p and the capacitance of a second cell (C_{m2}) were calculated by computer program on the basis of the simplified equivalent circuit proposed for mast cell degranulation (Zimmerberg et al., 1987).[3] If this circuit is applicable to virus-induced cell–cell fusion, G_p and C_{m2} could be calculated as described in Lindau (1991):

$$G_p = (\Delta Re^2 + \Delta Im^2)/\Delta Re \quad (1)$$

$$C_{m2} = (\Delta Re^2 + \Delta Im^2)/\omega \cdot \Delta Im, \quad (2)$$

where ΔRe and ΔIm are fusion-induced increments of the real and imaginary part of the pipette–cell admittance, respectively; $\omega = 2\pi f$; and f is the frequency of the stimulating sine wave. The beginning of fusion was detected automatically as the first point of a signal that exceeded twice the SD of a selected base line. To suppress the artifacts of fluid ejection close to a cell pair, base line segments were adjusted by filtering and subtracting filtered points from an initial data segment. A 5-Hz cut-off frequency, 9-order low pass digital Gaussian filter was used for this purpose.

The radius of an initial pore, r, was calculated as:

$$r = \frac{\pi\rho G_p + \sqrt{(\pi\rho G_p)^2 + 16\pi\rho h G_p}}{4\pi} \quad (3)$$

(modified from Hille, 1992), where ρ is the specific resistance of pipette solution (70.4 Ohm × cm), and h is the height of a baculovirus spike (~12 nm; Adams et al., 1977).

Kinetics. The waiting time (t_w) was measured from the onset of the pressure pulse to deliver acid until fusion pore appearance. The probability that a fusion pore has not yet appeared at time t was defined as $P(t) = 1 - N(t)/N_e$, where $N(t)$ is the number of pores that have formed by time t and N_e is the total number of experiments. A number of kinetic schemes were tested for goodness-of-fit. Best results were found with a parallel model (Appendix 1) with many identical elements and one unique step that was inspired by the approach of Hodgkin and Huxley (1952) for fitting ionic channel currents and the recent work of Blumenthal and colleagues on HA-mediated fusion (Blumenthal et al., 1996).

Curve Fitting and Statistical Evaluation. Experimental data were fit with the nonlinear Marquardt-Levenberg algorithm as implemented in software (Sigma-Plot; Jandel Scientific, Corte Madera, CA). Commercial software was used for statistical analysis (Sigma-Stat; Jandel Scientific), with a $P < 0.05$ level of significance. The one-sample Kolmogorov-Smirnov (KS) test was performed to determine the normality of data samples. The two-sample, nonparametric KS test was used for comparison of two samples of data. For the two-sample KS test, D_{max} was calculated as $D_{max} = \max |cdf_1 - cdf_2|$, where cdf_1 and cdf_2 are cumulative distribution functions of two data samples, and D_{tab} is a tabulated value ($P < 0.05$). The null hypothesis was rejected if D_{max} exceeded D_{tab} (Hays and Winkler, 1970).

Results

Fusion Pores Are Large, Variable, and Often Stable

To measure fusion pore conductance unambiguously, we used double whole-cell recording (Fig. 1). Electrophysiological parameters of individual, contacting baculovirus-infected Sf9 cells were measured: the resting membrane potential was −38 ± 13.4 mV (n = 7), membrane capacitance was 16.6 ± 5.2 pF (n = 33), input resistance was 1.8 ± 0.6 GOhm (n = 21), and series resistance was 4.8 ± 2.6 MOhm (n = 30). At the high time resolution (100 μs), our noise was half that of the signal of gap junctional channels with the conductance of 100 pS (Zimmerberg et al., 1995). In three experiments when such channels were observed, fusion was triggered after spontaneous electrical uncoupling (irreversible closure of gap junctional channels). Thus, the junctional conductance before fusion pore opening was undetectable (<100 pS).

In 31 of 33 experiments, slow perfusion of low pH solu-

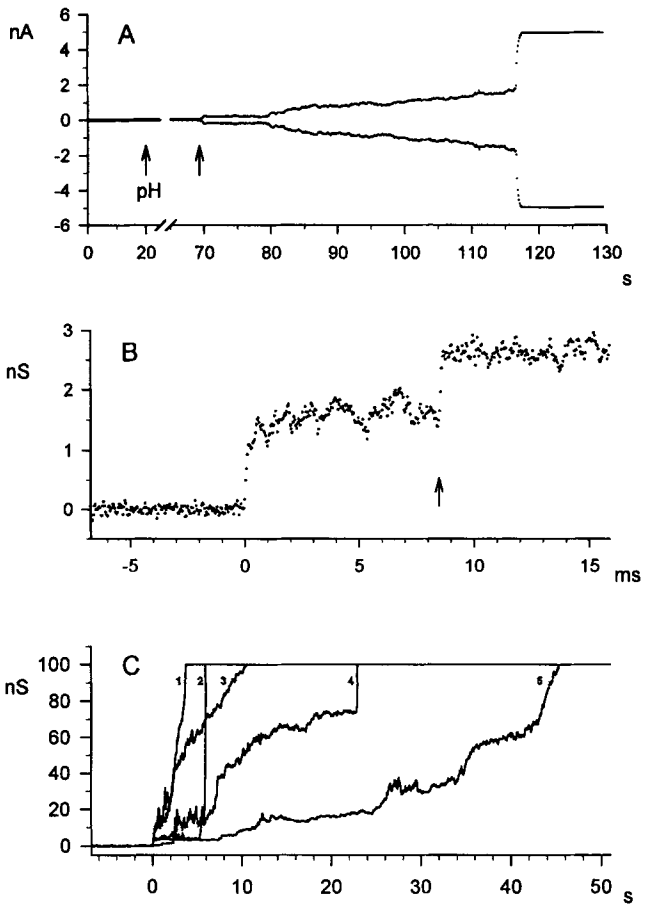

Figure 2. Time course of cell–cell fusion, studied by double whole-cell recording. (*A*) Perfusion of infected Sf9 cells with acid external solution (*first arrow* indicates the onset of slow perfusion) caused membrane fusion, displayed as the development of two symmetrical currents up to the saturation of the patch-clamp amplifiers. Fusion started at ~70 s of recording (*second arrow*). Transjunctional potential (50 mV) was constantly applied (V_1 = −50, V_2 = 0 mV). Zero time mark corresponds to the onset of DWCR. (*B*) Initial fusion pore at high time resolution (40-μs point-to-point interval). Zero time mark here and in *C* corresponds to initial fusion pore appearance. Second abrupt increment of junctional conductance occurred ~9 ms later (*arrow*). (*C*) Time course of the development of fusion-mediated intercellular conductance. Transjunctional currents from five such experiments as shown in *A* were converted into conductances and plotted together. Records 1–5 represent stages in fusion: a semistable phase (*2*, *4*, and *5*), a widening (*1*, *3*, and *5*), or final jump (*2* and *4*) to the saturation of amplifiers.

3. In the equivalent circuit for mast cells, only G_p and C_{m2} are taken into consideration (R_{s1} and C_{m1} are taken as compensated and R_{m1} and R_{m2} are negligible). For this case, the fusion-induced increment of the real part of Y (ΔRe) equals $(\omega C_{m2})^2/\{G_p\,[1+(\omega C_{m2}/G_p)^2]\}$ and the increment of the imaginary part of Y (ΔIm) equals $\omega C_{m2}/[1+(\omega C_{m2}/G_p)^2]$. Eqs. 1 and 2 can be derived from these expressions for ΔIm and ΔRe. Computer simulation of fusion pore widening using the parameters of a fusing Sf9 cell instead of a mast cell granule gave an excellent representation of the experimental admittance data, verifying the use of this equivalent circuit for viral fusion.

tion outside of a pair of cells induced a current flowing out of one cell into another (I_j in Fig. 1 *B*). This current reflected an increase in junctional conductance. I_j was recorded as the symmetrical signal from both patch-clamp amplifiers (Fig. 2 *A*). In control experiments, treating uninfected cells with low pH solution failed to induce any detectable I_j (n = 5). Junctional current never developed when infected cell pairs were perfused with physiological solution (pH 6.2 for insect cells). Thus, such increases in junctional conductance were induced by fusion.

A few characteristic stages of fusion could be determined, beginning with an abrupt opening of the fusion pore (Fig. 2 *B*). In 86% of the experiments, pore conductance subsequent to its opening was remarkably stable for a period of time that ranged from 0.01–70.80 s (median = 1.28 s). Surprisingly, in Sf9 cells infected with *Autographa californica* baculovirus, we did not observe any[4] flickering of the fusion pore, which is typical for exocytosis (Breckenridge and Almers, 1987; Curran et al., 1993) and HA-induced fusion (Spruce et al., 1989; Zimmerberg et al., 1994): each GP64-induced fusion pore opened irreversibly. After this first stage, the junctional conductance increased, typically through the development of additional abrupt pores (Fig. 2 *B*, *arrow*), an initial phase of pore widening, a semistable phase of conductance at the level of a few to tens of nS (Fig. 2 *C*; records *2*, *4*, and *5*), a second widening phase (Fig. 2 *C*; records *1*, *3*, and *5*), or a final jump (Fig. 2 *C*; records *2* and *4*) to the saturation of patch-clamp amplifiers.[5]

We characterized fusion pores in terms of their initial conductances (Fig. 3 *A*) and waiting times. Fusion pores had a broad distribution of initial conductance in the range of 300–1,700 pS with a mean of 1.0 ± 0.3 nS (Fig. 3, *B* and *C*), corresponding to initial pore radii of 1.8 ± 0.3 nm (Eq. 3).

Admittance Measurements and Double Whole-Cell Recordings Yield the Same Results

To validate the model-dependent admittance analysis and to collect data on fusion kinetics, fusion pore conductance

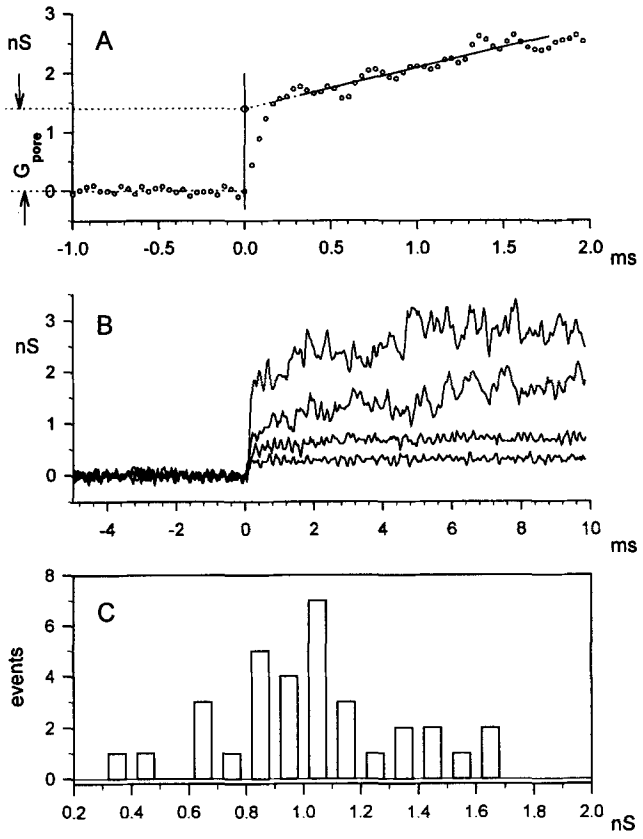

Figure 3. The conductance of the initial fusion pores, measured by double whole-cell recording. (*A*) The algorithm of calculation. A point, which is two times above an SD of base line segment, was assumed as first belonging to a fusion pore. Linear regression was applied to a "plateau" segment, situated after a fast transient of conductance. A regression line was extended to the intersection with a vertical line, drawn through a point that precedes fusion. It was assumed that initial pore conductance is equal to the distance between an intersection point and a mean of a base line segment. This approach helped to restore a signal, distorted by our instrumentation bandwidth and/or low pass filter of a cell. (*B*) A "family" of initial fusion pores. Four recordings from different experiments are shown. Zero time mark corresponds to the onset of fusion. (*C*) A histogram of initial conductance values.

during baculovirus-mediated Sf9 cell–cell fusion was calculated from admittance measurements. AM requires only one recording pipette, which facilitates the use of a second pipette for fast delivery of low pH solution. The algorithm for fusion pore calculation is described in Materials and Methods (Eq. 1).

Acidification of the external solution induced a change in the admittance of a pair of cells infected with baculovirus. Typically, the out-of-phase (imaginary) part of Y rises and reaches its maximum, whereas the in-phase (real) part reaches its maximum and then declines (Fig. 4 *A*), as expected.[3] In nineteen experiments, the pH of external solution was changed by slow perfusion, the same technique as used with DWCR. The general time course of baculovirus-induced fusion in these experiments, as well as in the experiments with fast delivery of acid (see below), revealed the same variability and common motifs: flicker-free initial fusion pore opening followed by other small abrupt con-

4. Our time resolution was mainly limited by the pipette-cell low pass filter of R_s and C_m. Flicker events much shorter than 75 μs could not be detected at all as a result of the analog low pass filter.

5. Second pores (Fig. 2 *B*) were seen in 52% of recordings. The dwell time of a second pore was 0.02–9.61 s with a median of 0.79 s. Detection of subsequent fusion pores was impeded by noise, which increased with each fusion pore. Third pores were observed in 14% of the experiments, and fourth pores were observed in 7% of experiments. Whether these current transients reflect changes in conductance of the same pore or are mediated by independent pores remains unclear. In comparison, for HA-induced cell–cell fusion, the lack of fluorescent aqueous dye flux despite multiple stepwise increases in G_p suggests the opening of multiple small pores (Zimmerberg et al., 1994). Fusion pore widening (nonabrupt increases of junctional conductance) could occur at any time, regardless of the number of fusion pore openings at the time widening started. Widening was seen in 76% of recordings and could be observed within a range of 0.013–36.70 s (median = 3.37 s). Unlike pore opening, fusion pore widening was reversible: junctional conductance came back to the level of the initial fusion pore in 7% of experiments. While widening of the initial fusion pore could continue beyond our ability to measure G_p, in most cases (62%), stabilization of junctional conductance occurred (range: 0.67–59.60 s; median = 9.8 s). Stabilization was often followed by a second widening of a pore (observed in 38% of recordings: range: 0.14–22.50 s; mean = 8.47 s) or a final jump of conductance beyond measurement (35% of recordings: range: 0.002–0.031 s, mean = 0.013 s).

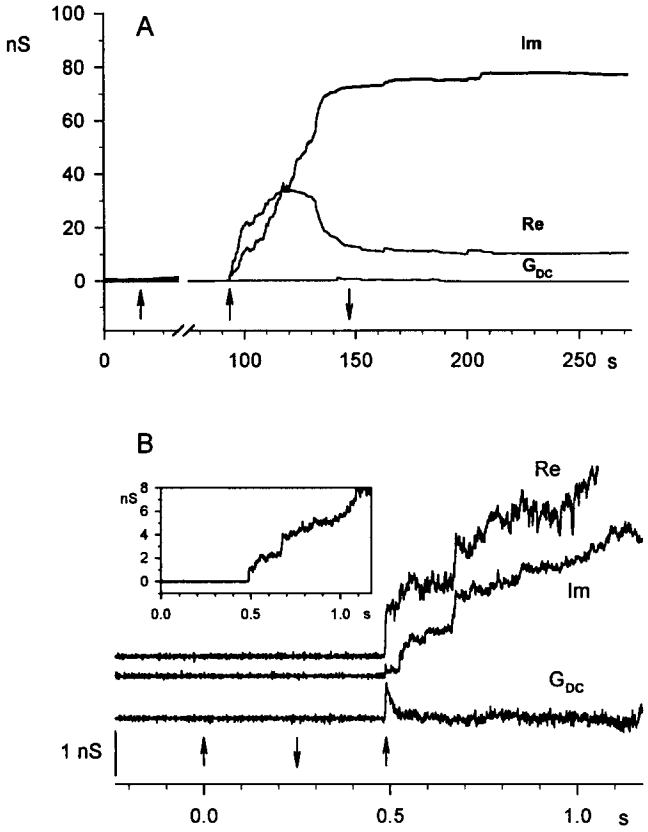

Figure 4. Baculovirus-induced Sf9 cells fusion, studied by time-resolved admittance measurement technique. (*A*) Perfusion of the experimental chamber with acid solution (*first* and *third arrows* indicate perfusion switching on and off) induces alterations in both real (*Re*) and imaginary (*Im*) components of pipette–cell admittance. The beginning of fusion is indicated by the second arrow. Direct current conductance (G_{DC}) shows no drastic change during fusion. Recording was started after pipette resistance and cell capacitance were electronically compensated (zero time mark). Between 25 and 75 s, readjustment of R_s compensation was done (not shown). (*B*) Acidification-induced alterations of Im, Re, G_{DC} are shown in fast time scale. Notice that in this experiment, fusion was triggered by ejection of acid solution from a delivery pipette (*first* and *second arrows* indicate a pressure pulse applied to a pipette). Signals were conditioned as discussed in Materials and Methods. Third arrow indicates the beginning of fusion. (*Inset*) Fusion pore conductance, calculated on the basis of the increments of Im and Re according to Eq. 1.

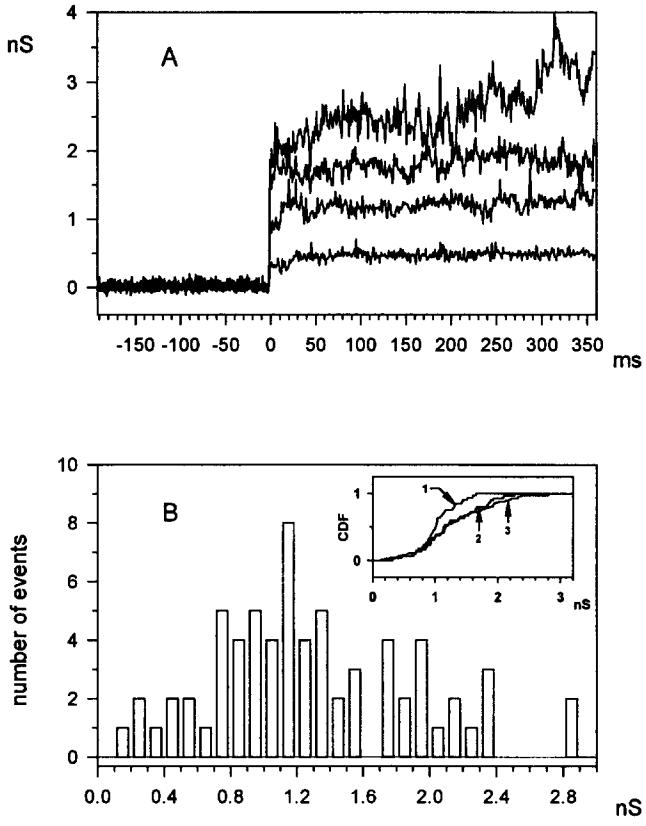

Figure 5. Time-resolved admittance measurements of the initial pore conductance. (*A*) Variability of initial conductance. Here, as in Fig. 3 *B*, four recordings were taken from different experiments. Zero time mark corresponds to a pore appearance. (*B*) A histogram of initial pore conductance. (*Inset*) Cumulative distribution function of initial pore conductance measured by DWCR technique after opening (*1*) and 1 ms later (*2*) vs one that was calculated using AM (*3*).

ductance jumps and/or pore widening, semistabilization of the junctional conductance, further pore growth, or a final jump to the microsiemen range (not shown).

Pores were detected as an abrupt increment of Re, coinciding with current discharge seen on the G_{DC} trace (Fig. 4 *B*). This current discharge is caused by the difference of the holding potential of cell 1 (−30 mV) and the membrane potential of cell 2, and it vanishes as C_{m2} charges to −30 mV. Unlike the short current transients used to calculate exocytotic and HA-induced fusion pores (Breckenridge and Almers, 1987; Spruce et al., 1991), current discharges in our experiments lasted longer since the fusing Sf9 cell's capacitance is much larger. A current transient was not observed when the holding potential of the first cell was close to the membrane potential of the second cell.

The initial pore conductance studied by AM showed the same characteristic features demonstrated by DWCR (Fig. 5 *A*). In AM, the mean value of the initial fusion pore conductance was 1.3 ± 0.6 nS (Fig. 5 *B*). To compare AM to DWCR, we prepared cumulative distribution functions for initial pore conductance (Fig. 5 *B*, *inset*, *arrows 1* and *3*). Kolmogorov-Smirnov statistics revealed a significant difference between these two samples (D_{max} = 0.301; D_{tab} = 0.289). We postulated that this difference was due to time resolution: DWCR (100 μs) is 10-fold faster than AM (1 ms). Unlike an ionic channel, a fusion pore can dilate immediately after abruptly opening, so the conductance of nonstable fusion pores measured by 1 ms after pore opening may be larger than its initial value. Comparison of initial fusion pore conductance measured by DWCR at 1 ms after pore opening (Fig. 5 *B*, *inset*, *arrow 2*) and calculated by AM (Fig. 5 *B*, *inset*, *arrow 3*) showed no significant difference (D_{max} = 0.091; D_{tab} = 0.289). In addition, we calculated the capacitance of the fusing cell, using admittance analysis (see Eq. 2). C_{m2} was equal to 17.5 ± 6.7 pF (n = 51). KS two-sample test showed no significant difference between this value and Sf9 cell capacitance, measured using the "C-slow" potentiometer of a patch-clamp amplifier (C_{m1} = 16.6 ± 5.2 pF; D_{max} = 0.113, D_{tab} = 0.302). The fact

that AM gave the same values of fusion pore conductance as DWCR validates the method of admittance analysis for the purpose of quantifying fusion pore conductance in this system.

Fusion Pores Form Quickly after Triggering

To collect data for kinetic analysis, the time of application of the acidic solution was controlled by pressure injection directly to the cell's surface. Fast delivery of acid solution to cell pairs allowed us to measure waiting times (t_w) from triggering to initial pore formation: t_w ranged from 0.2–3 s with a median value of 0.6 s (Fig. 6 *A*). To better delineate the deviations of t_w points from a single exponential, waiting times were displayed as a semilog survival plot (see Materials and Methods for details). A parallel model (Appendix 1) was devised to fit $P(t)$, the probability that a fusion pore has not yet appeared at time t (survival probability). The crux of the model is that after triggering, several independent identical elements move from non–fusion-permissive to fusion-permissive positions. Following this approach, we postulated that fusion is controlled by two species of activation elements: **a** and **b**. For fusion to occur, n independent **a**-type elements and one **b** element should move to their permissive state. Experimental waiting times were fit to the equation, derived on the basis of these assumptions (Eq. A3; see Appendix 1 for details). The following fitting parameters were obtained (given with standard error values): $n = 19.2 \pm 3.82$, $k_1 = 6.7 \pm 0.42\ s^{-1}$, $k_{-1} = 0.03 \pm 0.001\ s^{-1}$, $k_2 = 1.78 \pm 0.008\ s^{-1}$, where k_1, k_{-1} are forward and backward rate constants for **a**, respectively, and k_2 is the rate constant for **b**. The model gave a satisfactory fit to the data (Fig. 6 *A*; $R^2 = 0.9943$).

Discussion

Using both time-resolved admittance measurements and double whole-cell recording, we have characterized the fusion pore formed by the baculovirus envelope glycoprotein GP64, a fusion protein with a putative internal fusion peptide. Direct current measurements of syncytia formation allowed resolution of pore conductance opening at the speed of ~100 μs and confirmed calculations of fusion pore conductance using cell admittance data. The GP64-induced fusion pore differs from other fusion pores in four important ways: first, the initial fusion pore conductance is very large, ranging one order of magnitude larger than the smallest pores of HA-mediated cell–cell fusion (Spruce et al., 1991), mast cell exocytosis (Spruce et al., 1990), neutrophil exocytosis (Lollike and Lindau, 1995), or the single gap junctional channel conductance measured in the same cells with the same time resolution (Zimmerberg et al., 1995). Second, unlike other viral systems, the GP64-mediated fusion pore forms within seconds after acidification of the medium. Third, GP64 fusion pores, once open, do not completely close (they do not flicker). Fourth, the initial configuration of this pore complex could be relatively stable for up to 70 s, as judged by fusion pore conductance. Subsequent conductance growth is of two types: formation of more pores with abrupt rise times like the first pore, and variable increases in conductance that we interpret as widening of pores.

Kinetics of Fusion Pore Opening Are Fit by a Multielement Parallel Model

Electrophysiological study of HA-mediated fusion between transformed fibroblasts and erythrocytes reveals a lag between triggering and initial pore appearance with a median delay of 27 s at 30.4°C (Spruce et al., 1989). Waiting times were much shorter for GP64-induced fusion (median of 0.6 s). Attempts were made to find a reaction scheme that describes GP64-mediated fusion. We fit t_w to theoretical probability functions derived on the basis of sequential or branched reaction schemes, including up to five elements. None of them provided a satisfactory fit, defined as $R^2 > 0.99$ and SEM of parameters <20% of the mean (e.g., see Appendix 1). However, a model proposing that activation of fusion requires the parallel activity of many identical elements and one unique element provides a probability function that fits our data (see Fig. 6 *A*).

The short waiting times of baculovirus-induced fusion may reflect either the intrinsic properties of the GP64 molecule or a high surface density of fusion protein on infected cells. The dependence of t_w on surface density is well documented for HA-mediated fusion both by fluorescence dye transfer (Clague et al., 1991; Danieli et al., 1996) and by electrophysiological assays (Melikyan et al., 1995*a*). Delays between triggering and fusion have been attributed to the aggregation of trimers into fusion-competent complexes (Bentz, 1992). One can speculate that, under conditions of high GP64 surface density expected for cells that are producing viral envelope, fusion-competent aggregates are already formed (or their formation is fast and does not contribute to t_w), and the kinetics reflect downstream conformational changes of the complex. If so, the **a** element of our model could correspond to a fusion peptide, of which there is thought to be only one per monomer. Then the result of our fit for $n \sim 19 \pm 4$ would correspond to 15–23 monomers (five to eight trimers) of GP64 to provide enough fusion peptides to form a fusion-competent complex. In other words, fusion occurs only when such a complex exposes 15–23 hydrophobic peptides. The **b** element of the proposed scheme could represent a lipid-dependent step. Thus, delays could be generated even with preassembled fusion complexes.

Our model, which belongs to the same class as that of Hodgkin-Huxley (1952), is preferable for comparing different processes through its convenient parametrization. An interpretation of parallel model parameters as microscopic descriptions of a protein should be made with caution (Armstrong, 1981; Hille, 1992). However, the recently described homotetrameric structure of Shaker potassium channel (MacKinnon, 1991) gives hope that such model parameters (four "gating particles" for K^+ current) represent actual molecular events.

Implications for Models of Fusion Pore Structure

DWCR can be used for determining if viral fusion is leaky because with DWCR one can measure the electrical conductance of the wall of a fusion pore. Ionic leakage between the inside of the fusion pore and the extracellular space would be detected as unequal currents I_1 and I_2 (see Fig. 1 *B*). Since there was no detectable loss of transjunctional current, the pore wall was tight (detection limit was

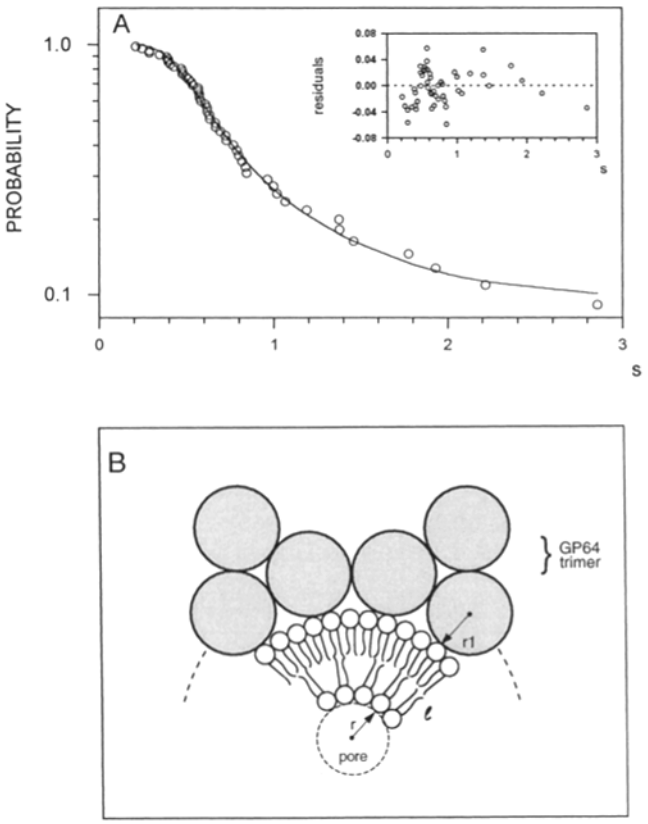

Figure 6. The analysis of fusion kinetics and hypothetical structure of the initial fusion pore. (*A*) Survival plot of waiting times between triggering of fusion and pore appearance. Experimental data points were fit to a theoretical probability function, derived on the basis of a parallel model. Residuals of fit are shown in the inset. (*B*) Cross-section diagram of a hypothetical baculovirus fusion pore complex showing only two GP64 trimers. The fusion pore is located in the middle of the complex. The number of GP64 monomers required to line a given pore radius can be estimated from $\pi/\arcsin[r1/(r+r1+l)]$, where $r1$ is the radius of a monomer, l is the thickness of a lipid layer (5 nm), and r is the radius of a fusion pore. If we approximate the shape of a GP64 monomer as a cylinder (Adams et al., 1977), then

$$r1 = \sqrt{\frac{M_W}{\pi h \nu N_A}}$$

where M_w is a molecular weight, h is a monomer height (~12 nm; Adams et al., 1977), v is a specific partial volume for proteins (0.74 g/cm^3), and N_A is Avogadro's number. For the mean conductance of GP64-induced initial fusion pores, these calculations yield $r1 \sim 2.0$ nm and 14 monomers in the circumference of the fusion pore complex.

<100 pS). For HA-mediated fibroblast–erythrocyte fusion, a similar conclusion was reached based on a comparison of G_p, measured with permeable vs impermeable solutions (Spruce at al., 1991).

On the basis of the quasi-abrupt opening of a small pore, the hypothesis was developed that the fusion pore opens initially as a proteinaceous pore, akin to a gap junction, and lipids add to the pore during its subsequent widening (Almers and Tse, 1990). Recent data from high resolution measurements of neutrophil degranulation have been interpreted to support this notion (Lollike et al., 1995). In contrast, the high degree of variability in fusion pore conductance in mast cells led us to hypothesize that the surface lining the fusion pore was lipidic in nature, and it represented a more fluid, lipid/protein complex (Zimmerberg et al., 1991). In the third hypothesis of membrane fusion, the stalk–pore model, the initial pore forms within a single hemifusion diaphragm (Chernomordik et al., 1995*a*, 1987; Monck and Fernandez, 1992; Nanavati et al., 1992). The last hypothesis is supported by the fact that a mutation of influenza hemagglutinin leads to hemifusion (Kemble et al., 1994; Melikyan et al., 1995*c*) and the correlation of lipid intrinsic curvature with inhibition and promotion of fusion (Chernomordik et al., 1995*b*). Regardless of the pathway, at later times semistable fusion pores represent coplanar, bent bilayers (Curran et al., 1993).

We can draw a speculative cartoon of an initial fusion pore that is made entirely of bent bilayers enclosed within a fusion complex formed by a ring of monomers from GP64 trimers. For such a structure, the number of GP64 monomers required to line a pore with a mean conductance of 1 nS is ~14 (Fig. 6 *B*). Adding the peripheral monomer of each trimer, the total number of monomers involved would be ~21. It is notable that this speculative number based upon the mean G_p value matches the number of monomers estimated in the kinetic model ($n \sim 19$). In contrast, to form initial fusion pores with a mean conductance of 1 nS with protein alone requires approximately six monomers (nine monomers total with three needed to pack a ring of three trimers). In this hypothetical proteinaceous initial fusion pore, variation of the number of monomers in the pore circumference could explain the wide distribution of initial conductance observed (Fig. 3 *C*). However, the predicted conductance histogram would be multipeaked, not continuous. Since G_p has a continuous distribution, the variation in pore conductance may result from a randomly variable distribution of membrane components lining the ion-conducting pathway of the fusion pore, as in Fig. 6 *B*.

For those ionic channels that are composed of aggregates of protein subunits, conductance tends to increase along with the number of their constitutive units (Unwin, 1989). Analogous to ionic channels, the difference in initial pore conductance mediated by HA and GP64 could be determined by a distinct subunit stoichiometry of corresponding fusion complexes. Three to four HA trimers were suggested for the initiation of fusion event (Danieli et al., 1996). However, six HA trimers were derived from the kinetic analysis of transitions of HA-mediated fusion pores from the initial size to a larger size (Blumenthal et al., 1996). Our model best fits a baculovirus-induced fusion pore composed of five to eight GP64 trimers. Of course, we do not know the actual geometric arrangement of GP64 within the fusion complex. Further analysis would benefit from knowledge of the chemical nature of the lining of the fusion pore.

Appendix 1

A parallel model was devised to fit $P(t)$. Suppose that fusion is controlled by two kinds of independent activation elements, **a** and **b**. For fusion to occur, several (n) **a** elements and one **b** element should move to their permissive

states, a^* and b^*, respectively. An acidification induces these transitions:

$$a \underset{k_{-1}}{\overset{k_1}{\rightleftarrows}} a^*$$

$$b \xrightarrow{k_2} b^*,$$

where k_1, k_{-1} are forward and backward rate constants for **a**, and k_2 is a rate constant for **b**. This reaction scheme leads to the following differential equations and solutions for a^* and b^*:

$$\frac{da^*}{dt} = k_1 a - k_{-1} a^*$$

$$\frac{db^*}{dt} = k_2 b$$

$$a^* = a_0 \left[k_1 \{\exp[t(k_1 + k_{-1})] - 1\} \cdot \frac{\exp[-t(k_1 + k_{-1})]}{k_1 + k_{-1}} \right] \quad \text{(A1)}$$

$$b^* = b_0 [1 - \exp(-k_2 t)], \quad \text{(A2)}$$

where a_0 and b_0 are amounts of **a** and **b** in nonpermissive state at $t = 0$. Let us define the probabilities for **a** and **b** to be in their permissive state, p_{a^*} and p_{b^*}, as a^*/a_0 and b^*/b_0. Assuming all elements are independent, $P(t)$, the probability that a fusion pore has not appeared at time t, equals $1 - (p_{a^*})^n \cdot p_{b^*}$. Dividing Eq. 4 by a_0 and Eq. 5 by b_0, yields:

$$P(t) = 1 - [k_1 \{\exp[t(k_1 + k_{-1})] - 1\} \cdot \frac{\exp[-t(k_1 + k_{-1})]}{k_1 + k_{-1}}]^n \cdot [1 - \exp(-k_2 t)]. \quad \text{(A3)}$$

Other attempts were made to find a reaction scheme that would fit our fusion kinetic data. Several sequential or branched schemes were tried unsuccessfully. For example, for HA-induced fusion, Bentz (1992) introduced the following reaction scheme:

$$\sigma_\omega \xrightarrow{K_{II}} II \xrightarrow{K_0} FP \xrightarrow{K_F} FS,$$
$$K_i \downarrow$$
$$IHA$$

where σ_ω denotes the number of fusion protein aggregates that are capable of forming intermembrane intermediates (II), IHA stands for inactivated HA, FP denotes fusion pores, and FS stands for fusion sites, which are structures that can be monitored by fluorescent dye redistribution. The author assumes (*a*) viral particle HA aggregates into preformed fusion-competent complexes, and (*b*) inactivation, if it occurs, starts from aggregated HA. The kinetic equation based on this reaction scheme fits experimental data for the fusion of influenza virus with ganglioside liposomes at low temperature.

We tried to adopt this reaction scheme to fit our waiting time distribution. Obviously, the last reaction step was not taken into consideration. Thus, the scheme reduces to:

$$A \xrightarrow{k1} II \xrightarrow{k2} FP,$$
$$k3 \downarrow$$
$$I$$

where A denotes aggregates and I denotes inactivated proteins. The probability function for such a reaction scheme was calculated as

$$P(t) = 1 - \frac{FP(t)}{A(0)},$$

which leads to:

$$P(t) = \frac{k1\,k2}{k2\text{-}k1\text{-}k3} \left\{ \frac{\exp[-k2\,(t - \Delta t)]}{k2} - \frac{\exp(k1 + k3)\,(-t + \Delta t) - 1}{k1 + k3} \right\},$$

where Δt is the offset correction on the time axis (see Fig. 6 *A*). After fitting t_w to this theoretical probability function (not shown), the following parameters were obtained: $\Delta t = 0.21 \pm 0.02$, $k1 = 3.26 \pm 2.02$, $k2 = 4.61 \pm 3.79$, and $k3 = 0.43 \pm 0.29$. Although the R^2 value for this fit was acceptable (0.9903), standard errors for parameter values were much higher than in the case of the parallel model.

We thank Drs. V. Ratinov, G. Melikyan, P. Blank, and A. Chrambach for valuable discussions, and Lynn Kelly for expert editorial assistance with the manuscript.

Received for publication 2 August 1996 and in revised form 14 October 1996.

References

Adams, J.R., R.H. Goodwin, and T.A. Wilcox. 1977. Electron microscopic investigations on invasion and replication of insect baculoviruses *in vivo* and *in vitro*. *Biol. Cell. (Ivry Sur Seine)*. 28:261–267.

Almers, W., and F.W. Tse. 1990. Transmitter release from synapses: does a preassembled fusion pore initiate exocytosis? *Neuron*. 4:813–818.

Alvarez de Toledo, G., and J.M. Fernandez. 1988. The events leading to secretory granule fusion. *In* Cell Physiology of Blood. R.B. Gunn and J.C. Parker, editors. The Rockefeller University Press, New York. 333–344.

Armstrong, C.M. 1981. Sodium channels and gating currents. *Physiol. Rev.* 61: 644–683.

Bentz, J. 1992. Intermediates and kinetics of membrane fusion. *Biophys. J.* 63: 448–459.

Blissard, G.W., and J.R. Wenz. 1992. Baculovirus gp64 envelope glycoprotein is sufficient to mediate pH dependent membrane fusion. *J. Virol.* 66:6829–6835.

Blumenthal, R., D.P. Sarkar, S. Durell, D.E. Howard, and S.J. Morris. 1996. Dilation of the influenza hemagglutinin fusion pore revealed by the kinetics of individual cell-cell fusion events. *J. Cell Biol.* 135:63–71.

Breckenridge, L.J., and W. Almers. 1987. Currents through the fusion pore that forms during exocytosis of a secretory vesicle. *Nature (Lond.)*. 328:814–817.

Chernomordik, L.V., G.B. Melikyan, and Y.A. Chizmadzhev. 1987. Biomembrane fusion: a new concept derived from model studies using two interacting planar lipid bilayers. *Biochim. Biophys. Acta*. 906:309–352.

Chernomordik, L., M.M. Kozlov, and J. Zimmerberg. 1995*a*. Lipids in biological membrane fusion. *J. Membr. Biol.* 146:1–14.

Chernomordik, L., E. Leikina, M.-S. Cho, and J. Zimmerberg. 1995*b*. Control of baculovirus gp64-induced syncytium formation by membrane lipid composition. *J. Virol.* 69:3049–3058.

Clague, M.J., C. Schoch, and R. Blumenthal. 1991. Delay time for influenza virus hemagglutinin-induced membrane fusion depends on hemagglutinin surface density. *J. Virol.* 65:2402–2407.

Curran, M.J., F.S. Cohen, D.E. Chandler, P.J. Munson, and J. Zimmerberg. 1993. Exocytotic fusion pores exhibit semi-stable states. *J. Membr. Biol.* 133: 61–75.

Danieli, T., S.L. Pelletier, Y.I. Henis., and J.M. White. 1996. Membrane fusion mediated by the influenza virus hemagglutinin requires the concerted action of at least three hemagglutinin trimers. *J. Cell Biol.* 133:559–569.

Fernandez, J.M., E. Neher, and B.D. Gomperts. 1984. Capacitance measurements reveal stepwise fusion events in degranulating mast cells. *Nature (Lond.)*. 312:453–455.

Hamill, O.P., A. Marty, E. Neher., B. Sakmann, and F.J. Sigworth. 1981. Improved patch-clamp technique for high resolution current recording from cells and cell-free membrane patches. *Pflügers Archiv. Eur. J. Physiol.* 391: 85–100.

Hays, W.L., and R.L. Winkler. 1970. Statistics: Probability, Inference, and Decision. Vol. 2. Holt, Rinehart, and Winston, New York. 320 pp.

Hille, B. Ionic Channels of Excitable Membranes. 1992. Second edition. Sinauer Associates Inc., Sunderland, MA. 607 pp.

Hodgkin, A.L., and A.F. Huxley. 1952. A quantitative description of membrane current and its application to conduction and excitation in nerve. *J. Physiol. (Lond.).* 117:500–544.

Hohmann, A.W., and P. Faulkner. 1983. Monoclonal antibodies to baculovirus structural proteins: determination of specificities by Western blot analysis. *Virology.* 125:432–444.

Joshi, C., and J.M. Fernandez. 1988. Capacitance measurements. An analysis of the phase detector technique used to study exocytosis and endocytosis. *Biophys. J.* 53:885–892.

Keddie, B.A., and L.E. Volkman. 1985. Infectivity difference between the two phenotypes of Autographa californica nuclear polyhedrosis virus: importance of the 64K envelope glycoprotein. *J. Gen. Virol.* 66:1195–1200.

Kemble, G.W., T. Danieli, and J.W. White. 1994. Lipid-anchored influenza hemagglutinin promotes hemifusion, not complete fusion. *Cell.* 76:383–391.

Lanzrein, M., N. Kasermann, R. Weingart, and C. Kempf. 1993. Early events of Semliki Forest virus-induced cell-cell fusion. *Virology.* 196:541–547.

Leikina, E., H. Ongun Onaran, and J. Zimmerberg. 1992. Acidic pH induces fusion of cell infected with baculovirus to form syncytia. *FEBS Lett.* 304:221–224.

Lindau, M. 1991. Time-resolved capacitance measurements: monitoring exocytosis in single cells. *Q. Rev. Biophys.* 24:75–101.

Lollike, K., N. Borregaard, and M. Lindau. 1995. The exocytotic fusion pore of small granules has a conductance similar to an ionic channel. *J. Cell Biol.* 129:99–104.

MacKinon, R. 1991. Determination of the subunit stoichiometry of a voltage-activated potassium channel. *Nature (Lond.).* 350:232–235.

Melikyan, G.B., W.D. Niles, and F.S. Cohen. 1995*a*. The fusion kinetics of influenza hemagglutinin expressing cells to planar bilayer membranes is affected by HA density and host cell surface. *J. Gen. Physiol.* 106:783–803.

Melikyan, G.B., W.D. Niles, V. Ratinov, M. Kaharnek, J. Zimmerberg, and F.S. Cohen. 1995*b*. Comparison of transient and successfully open fusion pores connecting hemagglutinin (HA) expressing cells to planar membranes. *J. Gen. Physiol.* 106:803–821.

Melikyan, G.B., J.M. White, and F.S. Cohen. 1995*c*. GPI-anchored influenza hemagglutinin induces hemifusion to both red blood cell and planar bilayer membranes. *J. Cell Biol.* 131:679–691.

Monck, J.R., and J.M. Fernandez. 1992. The exocytotic fusion pore. *J. Cell Biol.* 119:1395–1404.

Monsma, S.A., and G.W. Blissard. 1995. Identification of a membrane fusion domain and an oligomerization domain in the baculovirus GP64 envelope fusion protein. *J. Virol.* 69:2583–2595.

Nanavati, C., V. Markin, A. Oberhauser, and J.M. Fernandez. 1992. The exocytotic fusion pore as a protein-supported lipidic structure. *Biophys. J.* 63: 1118–1132.

Neher, E., and A. Marty. 1982. Discrete changes of cell membrane capacitance observed under conditions of enhanced secretion in bovine adrenal chromaffin cells. *Proc. Natl. Acad. Sci. USA.* 79:6712–6716.

Neyton, J., and A. Trautmann. 1985. Single channel currents of an intercellular junction. *Nature (Lond.).* 377:283–295.

Spruce, A.E., A. Iwata, J.M. White, and W. Almers. 1989. Patch clamp studies of single cell-fusion events mediated by a viral protein. *Nature (Lond.).* 342: 555–558.

Spruce, A.E., L.J. Breckenridge, A.K. Lee, and W. Almers. 1990. Properties of the fusion pore that forms during exocytosis of a mast cell secretory vesicle. *Neuron.* 4:643–654.

Spruce, A.E., A. Iwata, and W. Almers. 1991. The first millisecond of the pore formed by a fusogenic viral envelope protein during membrane fusion. *Proc. Natl. Acad. Sci. USA.* 88:3623–3627.

Tse, F.W., A. Iwata, and W. Almers. 1993. Membrane flux through the pore formed by a fusogenic viral envelope protein during cell fusion. *J. Cell Biol.* 121:543–552.

Turin, L., P.H. Behe, I.M. Plonsky, and A. Ya. Dunina-Barkovskaya. 1991. Hydrophobic ion transfer between membranes of adjacent hepatocytes. A possible role of tight junction structure. *Proc. Natl. Acad. Sci. USA.* 88: 9365–9369.

Unwin, N. 1989. The structure of ion channels in membranes of excitable cells. *Neuron.* 3:665–676.

Volkman, L.E., and P.A. Goldsmith. 1984. Budded Autographa californica NPV 64K protein: further biochemical analysis and effects of immunoprecipitation sample preparation conditions. *Virology.* 139:295–302.

White, J.M. 1992. Membrane fusion. *Science (Wash. DC).* 258:917–924.

Zimmerberg, J., M. Curran, F.S. Cohen, and M. Brodwick. 1987. Simultaneous electrical and optical measurement show that membrane fusion precedes secretory granule swelling during exocytosis of beige mouse mast cell. *Proc. Natl. Acad. Sci. USA* 84:1585–1589.

Zimmerberg, J., M. Curran, and F.S. Cohen. 1991. A lipid/protein complex hypothesis for exocytotic fusion pore formation. *Ann. NY Acad. Sci.* 635:307–317.

Zimmerberg, J., R. Blumenthal, D.P. Sarkar, M. Curran, and S.J. Morris. 1994. Restricted movement of lipid aqueous dyes through pores formed by influenza hemagglutinin during cell fusion. *J. Cell Biol.* 127:1885–1894.

Zimmerberg, J., S.S. Vogel, T. Whalley, I. Plonsky, A. Sokoloff, A. Chanturia, and L.V. Chernomordik. 1995. Intermediates in membrane fusion. *Cold Spring Harbor Symp. Quant. Biol.* LX:589–599.